

# Evaluating Lemon-Derived Biochar for Synthetic Dye Removal: A Green Approach to Water Treatment

Fawwaz Khalili<sup>1</sup>, Omar Alnasra<sup>1\*</sup>, Omar Almaani<sup>2</sup>, and Shrouq AlAzzeh<sup>1</sup>

<sup>1</sup> Department of Chemistry, Faculty of Science, The University of Jordan, Amman, Jordan.

<sup>2</sup> Department of Chemistry, Faculty of Science, Petra University, Amman, Jordan.

Received on 1 March 2025; Accepted on 15 December 2025

## Abstract

Synthetic cationic dyes, such as crystal violet (CV) and methylene blue (MB), are persistent water pollutants that pose toxicological risks and impair aquatic ecosystems, while conventional activated carbons remain relatively expensive and are not always derived from sustainable sources. There is a particular lack of systematic kinetic and thermodynamic data for commercially available lemon-derived charcoals used under near-neutral pH conditions relevant to water treatment. This study evaluates the adsorption performance of a lemon-derived charcoal (LC) adsorbent for effectively removing CV and MB from aqueous solutions. The adsorbent's physico-chemical characteristics were determined by Fourier transform infrared (FTIR) spectroscopy, X-ray diffraction (XRD), thermogravimetric analysis (TGA), and scanning electron microscopy (SEM), confirming the presence of functional groups (e.g., hydroxyl, carbonyl, and phenolic) and a porous microstructure crucial for dye binding. Operational factors, including adsorbent dosage, contact time, and temperature, were examined to optimize adsorption. Kinetic results indicated that both dyes followed a pseudo-second-order model, consistent with a chemisorption-controlled rate. Isotherm analyses demonstrated a predominantly monolayer adsorption mechanism compatible with the Langmuir model, yielding maximum dye removal efficiencies of 82.24% for CV and 77.37% for MB. Thermodynamic assessment revealed that CV adsorption is exothermic, while MB adsorption is endothermic. Overall, these findings underscore the potential of commercially available lemon-derived charcoal as an eco-friendly and cost-effective adsorbent for mitigating dye pollution in wastewater treatment systems.

© 2026 Jordan Journal of Earth and Environmental Sciences. All rights reserved

**Keywords:** lemon charcoal; crystal violet; methylene blue; water treatment; waste recycling

## 1. Introduction

The release of synthetic dyes, such as crystal violet (CV) and methylene blue (MB), from textile, pharmaceutical, and food industries is a significant source of water pollution. These cationic dyes are persistent, bioactive molecules that can cause eye and skin irritation, cyanosis, and potentially carcinogenic effects in humans and animals (Senthilkumar et al., 2005; Saeed et al., 2010; Li et al., 2016; Ibrahim et al., 2019). In surface waters, their intense color reduces light penetration, suppressing photosynthesis and disrupting aquatic food webs, which ultimately degrades water quality and ecosystem stability (Wang et al., 2019; Cheng et al., 2022). As global concerns about water quality and environmental sustainability continue to grow, there is an increasing demand for efficient and cost-effective methods to remove these pollutants from water sources (Bikram et al., 2023). Adsorption is recognized as a promising approach for the removal of dyes from aqueous solutions due to its simplicity, effectiveness, and versatility (Gupta and Suhas, 2009; Al-Jboor and Khalili, 2011; Alnasra and Khalili, 2023). Over the past decade, researchers have made substantial progress in exploring novel adsorbent materials to address the dye removal challenge. Among these materials, activated carbon derived from agricultural waste products has garnered attention for its affordability, sustainability, and remarkable

adsorption capabilities (Foo and Hameed, 2012; Öztürk and Bektaş, 2004).

Lemon charcoal, as a potential candidate in this context, is derived from lemon peels, which are often discarded as waste. Several studies have investigated the adsorption properties of lemon charcoal for various pollutants, showcasing its potential as a versatile adsorbent material (Foo and Hameed, 2012; Öztürk and Bektaş, 2004; Al-Qadri et al., 2024). The utilization of lemon charcoal as an adsorbent material not only offers a sustainable solution to waste management but also holds promise for efficient dye removal (Foo and Hameed, 2012; Ramutshatsha-Makhwedzha et al., 2022). The utilization of lemon peels in this study aligns with the global effort to minimize agricultural waste and repurpose it for environmental remediation. Lemon peels, often discarded as by-products of the citrus industry, are a valuable resource due to their high lignocellulosic content and bioactive compounds. This study demonstrates how these residues can be transformed into functional biochar, contributing to a circular economy model. Beyond lemon peels, future research should explore integrating other agricultural wastes, such as orange peels, banana skins, and sugarcane bagasse, to diversify potential adsorbent sources. Such efforts would not only reduce waste generation but also expand the scope of sustainable water

\* Corresponding author e-mail: o\_alsnasra@ju.edu.jo

treatment technologies. This research aims to contribute to the existing body of knowledge by examining the adsorption capacity of LC specifically for CV and MB, two dyes with distinct chemical properties. Understanding the adsorption behavior of lemon charcoal towards these dyes is crucial for its practical application in wastewater treatment and environmental remediation. Moreover, it provides an opportunity to explore the underlying mechanisms governing the adsorption process, contributing to a broader understanding of adsorption phenomena.

## 2. Experimental

### 2.1 Chemicals and Preparation of the Adsorbent

All chemicals used in this study were of analytical grade. Commercial lemon-wood charcoal in granular form was purchased from a local supplier in Amman, Jordan, and is marketed simply as "LC". CV and MB were analytical-grade dyes, obtained from Gain Chemical Company (GCC) and s.d. Fine-Chem Ltd., respectively. According to the 'manufacturers' specifications, both dyes have dye content  $\geq 90\%$  and were used as received without further purification. Hydrochloric acid (HCl, 37%) was purchased from Tedia, and sodium hydroxide pellets (NaOH) from Merck KGaA.

LC was supplied as a pre-carbonized lemon-wood charcoal produced industrially by slow pyrolysis in limited oxygen. The manufacturer did not disclose the exact operating temperature or provide specific BET surface area or pore volume data; therefore, information on microstructure and porosity was inferred from the XRD, SEM, and TGA analyses presented in Section 3.1, which are consistent with a high-temperature ( $>400^\circ\text{C}$ ) woody biochar (Tintner et al., 2018; Dittmann et al., 2022). In our laboratory, the charcoal was gently ground in a Mini-Philips mill, sieved to select particles with sizes between 125 and 250  $\mu\text{m}$ , rinsed several times with deionized water to remove fines and soluble impurities, and then oven-dried at  $105^\circ\text{C}$  for 24 h. No additional chemical activation or surface modification was applied, so that the adsorption performance reflects a readily available low-cost LC.

### 2.2 Instrumentation

A mini-Philips mining machine was employed to grind the adsorbent material. All mass measurements were conducted with precision using the RADWAG® AS 220 analytical balance. For LC characterization, a variety of advanced instruments were utilized. FTIR spectra were obtained using a Thermo-Nicolet NEXUS 670 FT-IR spectrophotometer. Thermal analysis, specifically TGA, was performed using a NETZCH STA 409 PG/PC thermal analyzer under a nitrogen atmosphere, with a heating rate of  $20^\circ\text{C}$  per minute over the temperature range of 0 to  $1000^\circ\text{C}$ . Powder X-ray diffraction (XRD) was conducted using a Philips 'X'Pert PW 3060 instrument, with controlled scanning parameters set at a rate of  $1^\circ/\text{min}$  over a  $2\theta$  range of  $2^\circ$  to  $60^\circ$ . The three-dimensional surface morphology was examined via scanning electron microscopy (SEM) using the 'NCFL's FEI QUANTA 600 FEG model. The concentrations of CV and MB in solution were determined spectrophotometrically using a METASH UV-Vis spectrophotometer model V-5100 equipped with a 1.0 cm quartz cell.

### 2.3 Calibration curves for dyes

In this study, calibration curves and their corresponding equations were derived by measuring the absorbance of standard solutions of CV and MB at specified concentrations. For CV, absorbance measurements were taken at a wavelength of 590 nm for solutions with concentrations ranging from 0.10 to 10.0 mg/L. For MB, absorbance was measured at 665 nm for solutions with concentrations between 1.0 and 15.0 mg/L. All calibration solutions were prepared in deionized water whose pH was adjusted to  $7.0 \pm 0.1$  using minimal volumes of 0.1 M HCl or NaOH, matching the pH employed in the equilibrium adsorption experiments. Calibration plots, along with regression equations and coefficients of determination ( $R^2$ ) are provided in Supplementary Figure S1 for both dyes. For any sample whose absorbance exceeded the linear range of the corresponding calibration curve, the solution was diluted with deionized water so that the final absorbance fell within the calibrated interval. Throughout this work, dye concentrations in aqueous solution are expressed in mg/L (for dilute aqueous solutions,  $1 \text{ mg/L} \approx 1 \text{ ppm}$ ).

### 2.4 Adsorption experiments

A one-factor-at-a-time optimization strategy was employed to determine the optimal conditions for the batch adsorption experiments. In a typical run, 25.0 mL of dye solution (CV or MB), with initial concentrations of 10 mg/L for CV and 30 mg/L for MB, was used, and the pH of the solutions adjusted to values between 4 and 8 for CV and 3 and 8 for MB, using 0.1 M HCl or NaOH. The adsorbent, lemon-wood charcoal, was added in varying amounts (0.010–0.90 g) to the solutions in 100 mL plastic bottles, followed by agitation at  $25^\circ\text{C}$  for 60 min. The effect of contact time was investigated separately by varying the contact time between 10 and 120 min. The suspensions were then filtered using nylon micro-filters (0.45  $\mu\text{m}$ ), and the concentration of unadsorbed dye in the filtrate was measured using the UV-Vis spectrophotometer. Adsorption isotherm experiments were also conducted at pH 7.0 and constant temperatures of 25.0, 35.0, and  $45.0^\circ\text{C}$  with initial dye concentrations ranging from 3 to 20 mg/L for CV and 5 to 60 mg/L for MB. For isotherm experiments, the suspensions were shaken for 60 min to reach equilibrium and then filtered. The removal percentage of dyes was calculated as a function of pH, adsorbent dose, contact time, and temperature. Unless otherwise stated, each experimental condition was repeated three times and the mean value is reported. Method blanks (deionized water only), LC-only controls without dye, and dye solutions passed through 0.45  $\mu\text{m}$  filters in the absence of LC were included in each batch to verify the absence of background signals and filtration losses at the measurement wavelengths.

Finally, kinetic and isotherm studies were conducted under optimal conditions for each dye to elucidate the characteristics of the adsorption reaction. Kinetic studies were carried out by monitoring dye uptake as a function of time (10–120 min) at fixed initial concentrations, while adsorption isotherms were examined at the concentration ranges specified above. The kinetic (PFO, PSO) and equilibrium (Langmuir, Freundlich, Dubinin–Radushkevich, and Temkin) models used in this work are widely reported in

the adsorption literature (Cheng et al., 2022; Gugushe et al., 2021; Mpupa et al., 2020).

### 2.5 Determination of the point of zero charge (pH<sub>pzc</sub>)

The point of zero charge (pH<sub>pzc</sub>) of LC was determined using the pH-drift method. A series of 50.0 mL 0.01 M NaCl solutions was prepared, and their initial pH (pH<sub>i</sub>) adjusted to the range 2.0–12.0 using 0.1 M HCl or 0.1 M NaOH. Then, 0.05 g of LC was added to each solution in 100 mL screw-cap bottles, and the suspensions were agitated at 25 ± 1 °C for 24 h. After equilibration, the final pH (pH<sub>f</sub>) was measured. The difference ΔpH = pH<sub>f</sub> – pH<sub>i</sub> was plotted as a function of pH<sub>i</sub>, and the pH<sub>pzc</sub> was taken as the pH<sub>i</sub> at which ΔpH = 0.

### 2.6 Data analysis

All batch adsorption experiments were performed in triplicate (n = 3). Model parameters for kinetic and equilibrium studies were obtained by least-squares linear regression of the corresponding linearized equations. In the figures, data points represent mean values and the error bars correspond to ±1 standard deviation. The goodness of fit for each model was evaluated by the coefficient of determination (R<sup>2</sup>).

### 2.7 Equilibrium and kinetic models

The equilibrium adsorption data were analyzed using the Langmuir, Freundlich, D–R, and Temkin isotherm models. In their non-linear forms, these models can be written as shown in Table 1. For parameter estimation, the corresponding linearized forms were used.

**Table 1.** Models for linear and non-linear sorption isotherms

Isotherm model	Non-linear equation	Linear equation	Reference
Langmuir	$q_e = \frac{q_m K_L C_e}{1 + K_L C_e}$	$\frac{C_e}{q_e} = \frac{1}{q_m K_L} + \left(\frac{1}{q_m}\right) C_e$	Langmuir, 1918
Freundlich	$q_e = K_F C_e^{1/n}$	$\text{Log } q_e = \log K_F + \frac{1}{n} \log C_e$	Freundlich, 1906
D-R	$q_e = q_m e^{-\beta \epsilon^2}$	$\ln q_e = \ln q_m - \beta \epsilon^2$	Dubinin, 1960
Temkin	$q_e = \frac{RT}{b_T} \ln(K_T C_e)$	$q_e = \frac{RT}{b_T} \ln C_e + \frac{RT}{b_T} \ln K_T$	Temkin, 1940

The following two models were used in kinetic evaluation to better understand how the dyes adsorb to LC sorbent:

Pseudo-first-order (PFO) [30]:

$$\ln(q_e - q_t) = \ln q_e - k_1 t \quad (3)$$

and pseudo-second-order (PSO) [21]:

$$\frac{t}{q_t} = \frac{1}{k_2 q_e^2} + \frac{t}{q_e} \quad (4)$$

## 3. Results and discussion

### 3.1. Physio-chemical properties of the adsorbents

The functional groups present on the LC were examined using FTIR spectroscopy. The analysis of the functional groups present on the surface of the LC was conducted using a potassium bromide (KBr) disk at a 10% ratio. The spectrum of the LC adsorbent, as illustrated in Figure 1, reveals that the predominant functional group specified in LC is as follows: A broad peak around 3413 cm<sup>-1</sup> indicates the stretching of the O–H bond in hydroxyl surface functional groups on the LC surface (Nuhanović et al., 2019; Kar 2020; Janu et al., 2021; Roy et al., 2022). This O–H group is associated with phenols, alcohols, and carboxylic acids found in the chemical components of lemon wood, such as lignin, cellulose,

hemicellulose, and organic acids (Šabanović et al., 2019). Low-intensity adsorption peaks at 2924 cm<sup>-1</sup> and 2854 cm<sup>-1</sup> suggest the presence of symmetric aliphatic C–H functional groups (CH<sub>2</sub> and CH<sub>x</sub>) (Nuhanović et al., 2019; Ankona et al., 2021; Sirico et al., 2021; Ramutshatsha-Makhwedzha et al., 2022). These peaks, are likely linked to carbohydrate groups such as methoxy, methylene, and methyl groups (Rožič et al., 2014; Šabanović et al., 2019). Additionally, a double peak between 2339 and 2362 cm<sup>-1</sup> is attributed to the stretching of CO<sub>2</sub> bonds (Stevens et al., 2008). A peak at 1841 cm<sup>-1</sup> indicates the presence of ester functional groups, and a C=O bond near 1703 cm<sup>-1</sup> likely originates from carbonyl groups (Alam et al., 2018; Hasan et al., 2021). The adsorption band in the range of 1613–1616 cm<sup>-1</sup> corresponds to C=O stretching in esters, quinones, and ketones, as well as to conjugated C=C bonds (Rožič et al., 2014; Senophiyah-Mary et al., 2019; Roy et al., 2022). A peak around 1438 cm<sup>-1</sup> suggests the presence of C–OH bonds (Alam et al., 2018), with similar peaks reported in studies on LC (Foroutan et al., 2021; Azadian and Gilani, 2023). Peaks in the range of 1315–1317 cm<sup>-1</sup> may be attributed to CH<sub>2</sub> bending (Mariño et al., 2015). Stretching vibrations of C–O bonds, possibly from carbohydrates, appear at the broad peak at 1236 cm<sup>-1</sup>. A small peak at 898 cm<sup>-1</sup> is likely due to C–H stretching in the aromatic structures of lignin (Li et al., 2014), while the band near 875 cm<sup>-1</sup> is associated with asymmetric stretching of CO<sub>3</sub><sup>2-</sup> (Al-Hosney and Grassian, 2005; Kalina et al., 2022; Mishra et al., 2023). Distinctive peaks between 617 and 780 cm<sup>-1</sup> correspond to C–H bending in phenyl rings (Stella Mary et al., 2016; Foroutan et al., 2021; Mishra et al., 2023).

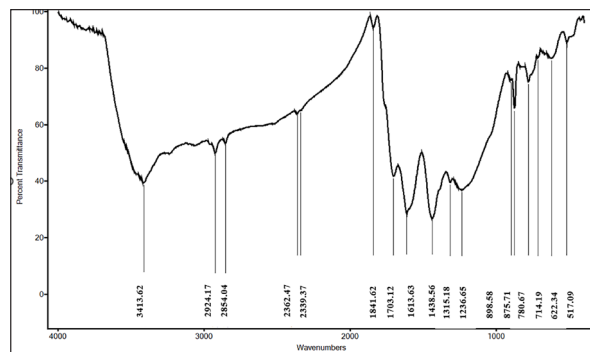


**Figure 1.** FTIR spectrum of LC for the investigation of the functional groups on the surface of the LC over a scanning range between 400 and 4000 cm<sup>-1</sup>

The thermogram in Figure 2a shows an initial mass loss below 200°C, which is attributed mainly to the desorption of physically adsorbed water and light volatile compounds. A further weight loss between approximately 200 and 400°C is associated with the decomposition of residual oxygen-containing surface groups and partially carbonized fragments remaining in the commercial charcoal. A more gradual mass loss between about 400 and 600°C likely reflects further dehydrogenation and condensation of aromatic structures. At higher temperatures, from 700 to 1000°C, the decomposition of inorganic carbonates (e.g., CaCO<sub>3</sub>) and other mineral constituents contributes to the residual mass changes, leaving a predominantly carbonaceous and mineral residue (Gomide et al., 2020; Dittmann et al., 2022). TGA was used here to verify that LC is thermally stable under

the conditions employed for adsorption experiments and to obtain additional information on the degree of carbonization and ash content.

The crystal phase and microstructure of the synthesized LC were validated through XRD, with the diffractographic pattern providing a definitive confirmation of a broad background (Figure 2b), indicating a predominantly amorphous structure in the adsorbent with at least four sharp crystalline peaks. The range from  $2\theta = 2.00^\circ$  to  $2\theta = 15.00^\circ$  corresponds to the micro-crystallographic features of biochar-type adsorbents (Danish et al., 2018). Peaks at  $2\theta = 15.22^\circ, 23.30^\circ, 24.71^\circ, 30.36^\circ, 36.24^\circ, 38.36^\circ, 39.66^\circ, 43.40^\circ, 47.76^\circ,$  and  $48.74^\circ$  are attributed to the crystalline graphite structure, while the peak at  $29.65^\circ$  is due to  $\text{CaCO}_3$  in LC and the crystalline graphite-like structure (Xie et al., 2014;

Jafri et al., 2018; Tintner et al., 2018; Oruç et al., 2019; Kar, 2020; Gabhi et al., 2020; Poonam and Kumar, 2020; Surya and Michael, 2021; Pérez et al., 2023).

The SEM images revealed that LC has a well-developed, irregular, and porous structure with many cavities. These images confirm that the wood cell and porosity morphologies remain prominent in the final biochar, with the adsorbent retaining much of the original wood cell structure. Moreover, the outer surface features varying pore sizes formed during pyrolysis. In Figure 2c (1000x magnification), the adsorbent shows wide and thick particles revealing characteristic wood structures, aligning with literature findings (Gomide et al., 2020). Figure 2d (4000x magnification) shows diverse pore sizes and shapes, indicating a high surface area (Kütahyalı and Eral, 2010; Azadian and Gilani, 2023).

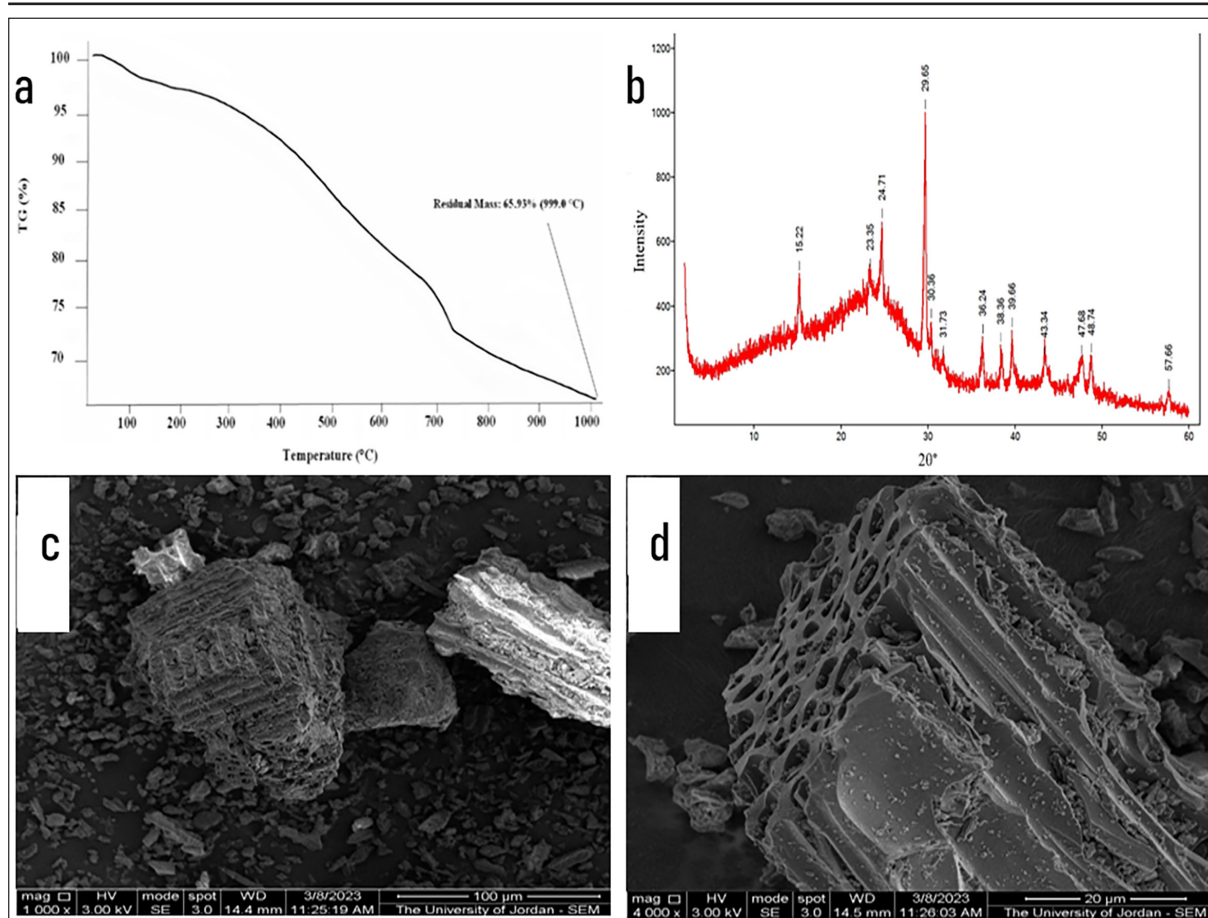


Figure 2. (a) TGA thermogram, (b) XRD spectrum, (c)–(d) SEM image

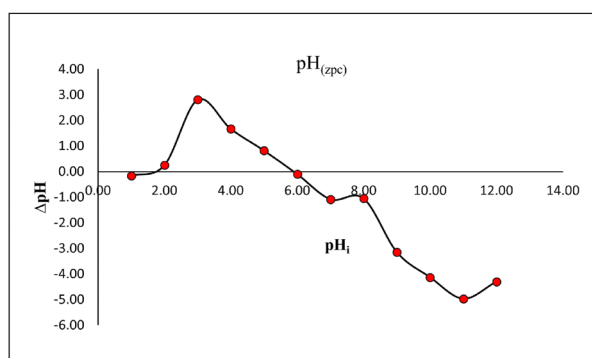


Figure 3. Determination of  $\text{pH}_{\text{zpc}}$  of LC by the pH-drift method. The intersection of the curve ( $\Delta\text{pH} = \text{pH}_f - \text{pH}_i$ ) with  $\Delta\text{pH} = 0$  occurs at  $\text{pH} \approx 6$ .

### 3.2. Evaluation of the adsorption performance of LC

#### 3.2.1. Adsorption experiment studies

The solution pH strongly influences dye adsorption because it controls both the adsorbent surface charge and the ionization state of the dye molecules (Baloo et al., 2021; Gupta et al., 2021). In the present study, the removal of CV and MB was examined over pH 3–8, and only minor variations in uptake ( $< 5\%$ ) were observed, indicating weak pH dependence (Supplementary Material, Figure S2). Both dyes remain cationic across these ranges—their ionizable functional groups (tertiary amine for CV, dimethylamino for MB) are protonated under neutral and mildly basic conditions, giving them a permanent positive charge. In contrast, LC possesses oxygen-containing surface groups (carboxyl,

phenolic, and lactonic) that progressively deprotonate above pH 3–4, imparting a net negative zeta potential to the surface (Rožič et al., 2014; Šabanović et al., 2019). Consequently, strong electrostatic attraction between positively charged dye molecules and the negatively charged LC surface is maintained throughout the investigated pH window. Only at pH > 8 would surface deprotonation saturation and hydroxide competition begin to reduce adsorption, but such conditions were not examined here. This mechanistic explanation aligns with prior studies on citrus-derived biochars and peels, which reported nearly constant adsorption of cationic dyes at neutral pH regions due to dominant electrostatic and  $\pi$ - $\pi$  stacking interactions (Senthilkumar et al., 2005; Foroutan et al., 2021; Ramutshatsha-Makhwedzha et al., 2022). Accordingly, pH 7.0 was selected for subsequent experiments as representative of natural and treated waters. As shown in Figure 3, the  $pH_{pzc}$  of LC was 6. Thus, the LC surface is expected to be positively charged at pH < 6 and predominantly negatively charged at pH > 6. Since the adsorption experiments were conducted mainly at pH 7.0 (>  $pH_{pzc}$ ), electrostatic attraction between the cationic dyes (CV and MB) and negatively charged LC surface sites is favored, which is consistent with the high removal efficiencies observed.

The adsorbent dosage is another critical operational variable. The effect of LC mass (0.01–0.90 g) on the uptake of CV and MB is presented in Figure 4. For both dyes, the percentage removal increased markedly with increasing LC mass and reached a plateau at 0.10 g, at which the adsorbent became effectively saturated and further increases in dosage produced only marginal additional removal. The slight decrease in the uptake expressed as  $q_e$  (mg g<sup>-1</sup>) at higher dosages arises from the lower driving force per unit mass at constant initial dye concentration. On this basis, an LC mass of 0.10 g was selected for all subsequent experiments.

Contact time was then optimized. Adsorption of both dyes on LC was very fast, with most of the uptake occurring within the first few minutes and no significant changes observed up to 120 min (Supplementary Material, Figure S3). To ensure that equilibrium was fully attained under all investigated conditions, a contact time of 60 min was adopted for the kinetic, isotherm, and thermodynamic studies.

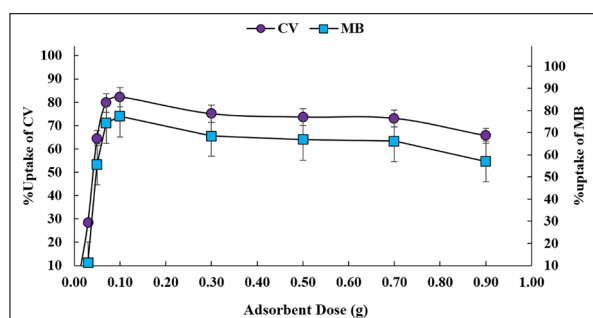
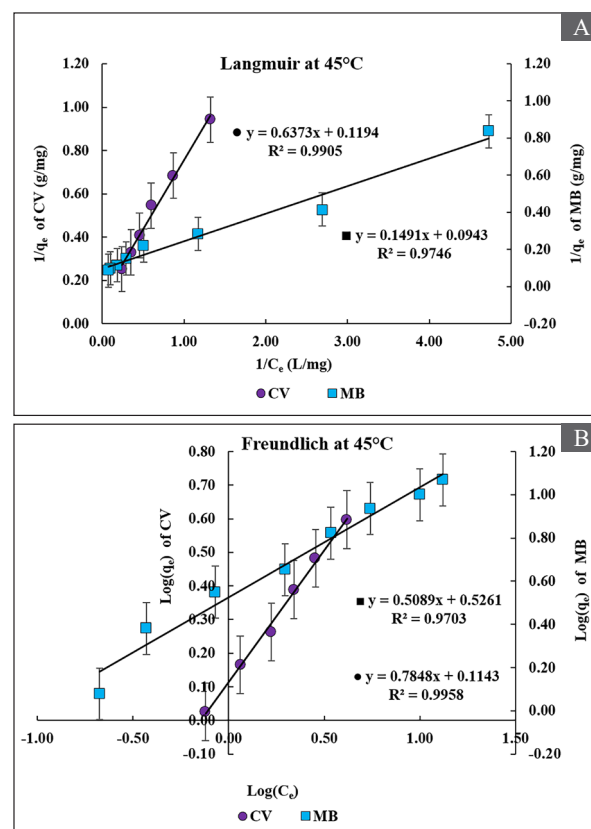


Figure 4. Effect of adsorbent dose on % uptake of CV and MB on LC

### 3.2.2. Isotherms data studies

Equilibrium adsorption data for CV and MB were interpreted using the Langmuir, Freundlich, D–R, and Temkin models, which respectively describe monolayer adsorption on homogeneous sites, multilayer adsorption

on heterogeneous surfaces, adsorption on energetically non-uniform sites, and adsorbate–adsorbent interactions (Langmuir, 1918; Freundlich, 1906; Dubinin, 1960). Isotherms were obtained at 25, 35, and 45 °C, and representative linear plots at 45 °C are shown in Figure 5. For both dyes, the equilibrium data fitted the Langmuir model very well (Figure 5a), indicating predominantly monolayer coverage, while the good agreement with the Freundlich and Temkin models (Figure 5b) reflects surface heterogeneity and non-negligible adsorbate–adsorbent interactions. The D–R model provided additional insight into the mean adsorption energy ( $E$ ) and supported a predominantly physisorption-controlled process (Fig. 4c). The isotherms for the CV and MB dyes were studied at 25, 35, and 45 °C. The obtained data were assessed using the R<sup>2</sup> coefficient, determined from the linear fits of the isotherm models. The isotherms were plotted as an illustrative example at 45 °C (Figure 5) for both dyes. Figure 5a showed excellent agreement with Langmuir for both CV and MB dyes, indicating the presence of a monolayer and homogeneous adsorption sites. Also Figure 5b shows excellent fitting with the Freundlich model, suggesting the presence of heterogeneous sites for both dyes. The D-R model showed relatively good fit and supports the notion that LC contains both homogeneous and heterogeneous sites (Figure 5c).



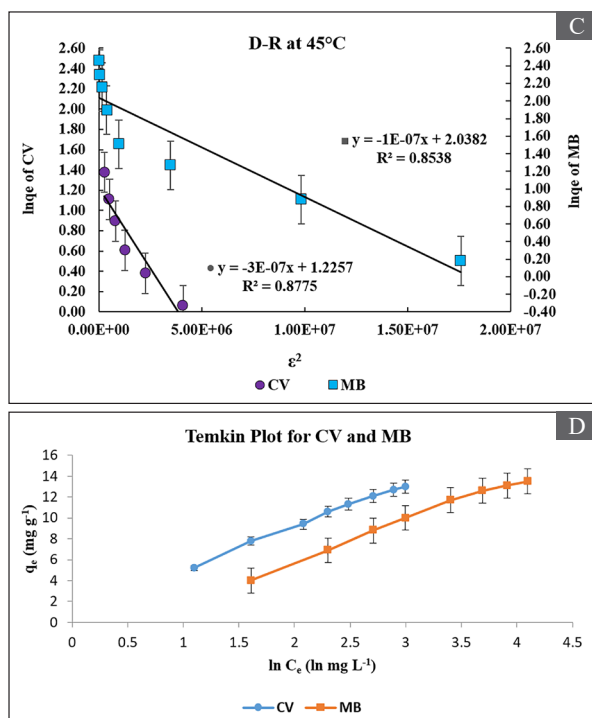


**Figure 5.** a) Langmuir b) Freundlich c) D-R d) Temkin models for CV and MB at 45 °C.

Table 1 presents adsorption isotherm parameters for the removal of CV and MB dyes using LC at different temperatures. For CV, the Langmuir isotherm showed the highest correlation coefficient ( $R^2$ ) values, particularly at 25 and 35 °C ( $R^2 = 0.991$  and  $0.993$ , respectively), suggesting monolayer adsorption as the dominant mechanism. The maximum adsorption capacity ( $q_m$ ) increased with temperature, indicating an endothermic process. The Langmuir separation factor ( $RL$ ) values ranged from 0 to 1, indicating favorable adsorption. The Freundlich isotherm also showed high  $R^2$  values, indicating the possibility of heterogeneous adsorption. Freundlich constant ( $n$ ) values greater than 1 indicate favorable adsorption conditions. In the D–R isotherm, the adsorption energy ( $E$ ) was below 8 kJ/mol, implying a physical adsorption mechanism. The Temkin model provided a good fit across all temperatures, with  $R^2$  values exceeding 0.98, highlighting the influence of adsorbent-adsorbate interactions.

For MB, the Langmuir model also fitted the equilibrium data well at all three temperatures, with the highest  $R^2$  observed at 45 °C ( $R^2 = 0.975$ ). The Langmuir  $q_m$  value estimated at 25 °C is markedly higher than those obtained at 35 and 45 °C, leading to an apparent decrease from 25 to 35 °C followed by a slight increase from 35 to 45 °C. This non-monotonic behavior should be interpreted cautiously. Because the 25 °C isotherm was constructed over a relatively narrow  $C_e$  range and exhibits very high  $R^2$ , small experimental uncertainties in  $C_e$  can strongly affect the extrapolated  $q_m$  while leaving  $R^2$  almost unchanged. Within the experimental scatter, the  $q_m$  values at 35 and 45 °C are of the same order of magnitude and consistent with the positive  $\Delta H^\circ$  obtained from the thermodynamic analysis, indicating that MB adsorption remains favorable at all three temperatures rather than being strongly enhanced specifically at 25 °C. The Langmuir separation factor ( $RL$ ) values for MB remained between 0 and 1 at all temperatures, confirming favorable adsorption. Freundlich isotherm results

also showed high  $R^2$  values, indicating adsorption on a heterogeneous surface, and the  $n$  values  $> 1$  reflect favorable adsorption conditions. The D–R model yielded adsorption energies  $E < 8$  kJ mol $^{-1}$ , consistent with a process dominated by physical adsorption, while the Temkin model gave good correlations ( $R^2 > 0.97$ ), highlighting the role of adsorbent-adsorbate interactions.

The previous results indicate that adsorption capacity and isotherm model fit vary with temperature for CV and MB. For both dyes, the Langmuir and Freundlich models consistently provided the best description of the equilibrium data, suggesting the coexistence of monolayer adsorption on relatively homogeneous sites and additional uptake on heterogeneous surface sites. For CV, the increase in  $q_m$  with temperature is consistent with the thermodynamic analysis and supports an endothermic adsorption process. For MB, the non-monotonic trend in  $q_m$  (higher value at 25 °C followed by a decrease at 35 °C and a slight increase at 45 °C) should be interpreted cautiously in light of the limited  $C_e$  span and resulting sensitivity of the extrapolated  $q_m$  at 25 °C. Overall, the isotherm analysis confirms that LC is an effective adsorbent for both CV and MB over the investigated temperature range, with adsorption primarily governed by physical interactions and surface heterogeneity.

To place the LC performance in context, it is useful to compare the present results with other citrus-derived and lignocellulosic adsorbents reported in the literature. Activated carbons and engineered biochars prepared from lemon and other citrus wastes often exhibit higher Langmuir capacities for cationic dyes under strongly optimized or chemically activated conditions (Foroutan et al., 2021; Ramutshatsha-Makhwedzha et al., 2022; Mishra et al., 2023). By contrast, the as-received lemon-wood charcoal used in this work, operated at near-neutral pH without additional activation, shows moderate capacities but achieves effective removal of both CV and MB with simple processing and low chemical input. This places LC among the class of low-cost, readily available sorbents whose main advantages are sustainability, ease of use, and operation under environmentally relevant conditions, rather than maximized capacity alone.

#### Kinetic studies

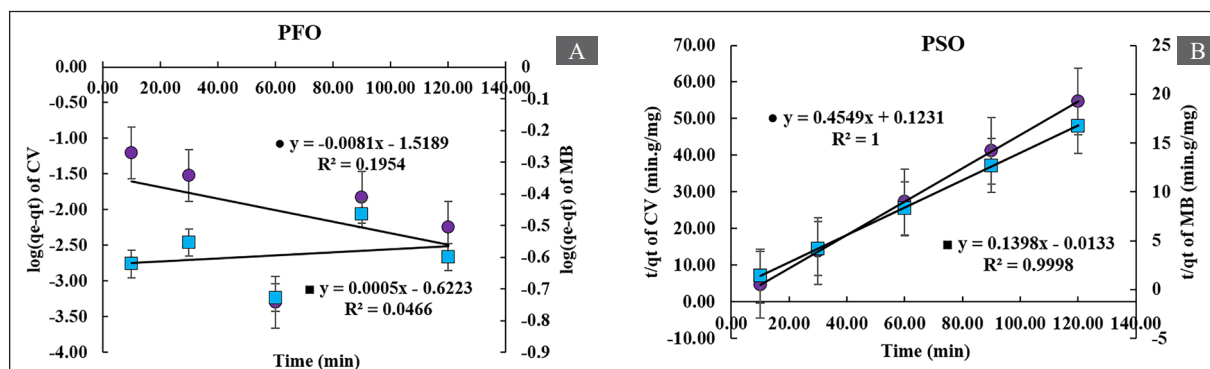
Pseudo-first-order (PFO) and pseudo-second-order (PSO) kinetic equations were used to describe the kinetic characteristics that control mechanisms of adsorption processes, such as mass transfer and chemical reactions. In pseudo-second-order reaction kinetics, the kinetic data from solid/solution sorption systems are described and correlated using this mathematical expression, which is currently the most widely used. By comparing the experimental  $q_e$  values with the calculated PSO kinetic plots, it is possible to determine the viability of this model. CV shows excellent fitting to PSO with  $R^2$  of one (Figure 6), while it shows very poor correlation coefficient of 0.1954 for PFO. This means that the rate determining step in the adsorption of CV into LC involve a chemisorption process. Similarly, MB showed excellent agreement with PSO and very poor one with PFO. Also this means that the rate determining step in the adsorption of MB into LC is a chemisorption step.

**Table 1.** Langmuir, Freundlich, D-R isotherm, and Temkin parameters for LC towards CV and MB, at different temperatures.

CV														
T(°C)	Langmuir Isotherm				Freundlich Isotherm			D-R Isotherm				Temkin Isotherm		
	R <sup>2</sup>	q <sub>m</sub> (mg/g)	K <sub>L</sub> (L/mg)	R <sub>L</sub>	R <sup>2</sup>	n (g/L)	K <sub>F</sub> (mg/g)	R <sup>2</sup>	B (mol <sup>2</sup> /kJ <sup>2</sup> )	q <sub>m</sub> (mg/g)	E (kJ/mol)	R <sup>2</sup>	K <sub>T</sub> (L/g)	b <sub>T</sub> (kJ/mol)
25.0	0.991	2.76	14.92	0.51	0.966	3.40	2.53	0.875	1.70 E-08	2.85	5.42	0.982	0.07	1.44
35.0	0.993	3.18	1.00	0.74	0.984	3.32	1.10	0.784	2.07 E-08	2.41	4.92	0.991	0.11	1.38
45.0	0.893	8.38	0.19	0.86	0.996	1.27	1.30	0.878	3.17 E-07	3.41	1.26	0.999	0.29	4.72

MB														
T(°C)	Langmuir Isotherm II				Freundlich Isotherm			D-R Isotherm				Temkin Isotherm		
	R <sup>2</sup>	q <sub>m</sub> (mg/g)	K <sub>L</sub> (L/mg)	R <sub>L</sub>	R <sup>2</sup>	n (g/L)	K <sub>F</sub> (mg/g)	R <sup>2</sup>	B (mol <sup>2</sup> /kJ <sup>2</sup> )	q <sub>m</sub> (mg/g)	E (kJ/mol)	R <sup>2</sup>	K <sub>T</sub> (L/g)	b <sub>T</sub> (kJ/mol)
25.0	0.900	341.4	0.014	0.38	0.966	0.75	4.39	0.875	4.54 E-07	16.88	1.05	0.992	6.309E-03	18.98
35.0	0.936	4.31	1.00	0.63	0.985	0.56	0.06	0.784	5.71 E-06	9.88	2.96	0.975	2.256E+05	24.02
45.0	0.975	10.60	0.63	0.86	0.996	2.24	3.71	0.878	9.76 E-08	6.29	2.26	0.988	0.1248	9.68



**Figure 6.** a) PFO b) PSO for the adsorption of CV and MB on LC

**Table 2.** Kinetic parameters for CV and MB adsorption on LC at 25 °C

CV			
Experimental qe = 2.200 (mg/g)			
Model	R <sup>2</sup>	k	Calculated qe (mg/g)
PFO	0.1954	k1= 1.87×10-2 min-1	0.028
PSO	1.0000	k2=5.96×10-1 g (mg.min)-1	2.198

MB			
Experimental qe = 7.189 mg/g			
Model	R <sup>2</sup>	k	Calculated qe mg/g
PFO	0.0443	k1= -1.38×10-3 min-1	0.030
PSO	1.0000	k2=1.19 g (mg.min)-1	7.189

Table 2 summarizes the kinetic parameters obtained for CV and MB with excellent agreement between experimental qe and calculated qe. It was 2.200 and 2.198 for CV, respectively, while for MB the values were 7.191 and 7.189, respectively. Also, it showed that the rate constant k2 (PSO) for MB is greater than that for CV. This means the rate of uptake for MB is larger than that of CV.

**Thermodynamics**

Thermodynamic parameters were evaluated from batch adsorption experiments conducted at initial dye concentrations of 10 mg/L for CV and 30 mg/L for MB, using equilibrium data obtained at 25, 35, and 45 °C. For each dye and temperature, the distribution coefficient was calculated as  $K_d = q_e/C_e$  (L g<sup>-1</sup>). The standard Gibbs free energy change was then obtained from  $\Delta G^\circ = -RT \ln K_d$ , where (R) is the

universal gas constant, and (T) is the absolute temperature. The enthalpy and entropy changes were determined from the ‘van’t Hoff relationship  $\ln K_d = \Delta S^\circ/R - \Delta H^\circ/(RT)$  by plotting (ln Kd) versus (1/T) and performing linear regression. Table 3 shows the resulting thermodynamic parameters for CV and MB at different temperatures. These parameters offer insights into the feasibility, spontaneity, and thermal effects of the adsorption processes. The ln Kd values for CV decreased with increasing temperature, indicating reduced adsorption affinity at higher temperatures. The negative  $\Delta G^\circ$  values across all temperatures confirm that the adsorption process is spontaneous, with  $\Delta G^\circ$  decreasing as temperature increases. This suggests that higher temperatures weaken the spontaneity of adsorption, possibly due to desorption effects or decreased adsorbent-adsorbate interactions. The negative

$\Delta H^\circ$  value (-148.19 kJ/mol) indicates that the adsorption of CV onto LC is exothermic. The negative  $\Delta S^\circ$  value (-0.46 kJ/mol·K) suggests decreased randomness at the solid-liquid interface during adsorption, consistent with dye molecules being immobilized on the LC surface. For MB, the  $\ln K_d$  values increased with temperature, reflecting enhanced adsorption affinity at elevated temperatures. The  $\Delta G^\circ$  values are negative at all temperatures, confirming the spontaneous nature of the adsorption. Furthermore, the magnitude of  $\Delta G^\circ$  becomes more negative with increasing temperature, indicating greater spontaneity at higher temperatures. The positive  $\Delta H^\circ$  value (39.90 kJ/mol) demonstrates that the adsorption of MB is endothermic, implying that increased temperature facilitates the adsorption process. The positive

$\Delta S^\circ$  value (0.14 kJ/mol·K) indicates increased randomness at the solid-liquid interface during adsorption, possibly due to the displacement of water molecules by MB onto the adsorbent surface. The thermodynamic analysis reveals contrasting behaviors for CV and MB adsorption. While CV adsorption is exothermic and less favorable at higher temperatures, MB adsorption is endothermic and improves with temperature. These differences may stem from the distinct physicochemical interactions between each dye and the LC. The negative  $\Delta G^\circ$  values for both dyes highlight the viability of the biochar as an effective adsorbent for removing CV and MB from aqueous solutions, although the optimal temperature conditions differ for each dye.

**Table 3.** Thermodynamic parameters for CV and MB at different temperatures

CV						
T (°K)	1/T (°K <sup>-1</sup> )	$\ln K_d$	$K_d$	$\Delta G^\circ$ (kJ/mol)	$\Delta S^\circ$ (kJ/mol)	$\Delta H^\circ$ (kJ/mol)
298.15	0.0034	4.23	68.72	-11.46	-0.46	-148.19
308.15	0.0032	3.54	34.47	-6.90		
318.15	0.0031	0.45	1.57	-2.32		
MB						
T (°K)	1/T (°K <sup>-1</sup> )	$\ln K_d$	$K_d$	$\Delta G^\circ$ (kJ/mol)	$\Delta S^\circ$ (kJ/mol)	$\Delta H^\circ$ (kJ/mol)
298.15	0.0034	1.01	2.75	-2.20	0.14	39.90
308.15	0.0032	1.16	3.19	-3.61		
318.15	0.0031	2.03	7.16	-5.03		

#### Proposed adsorption mechanism

The combined characterization and adsorption results suggest that multiple interaction mechanisms contribute to the uptake of CV and MB on LC. FTIR analysis (Figure 1) indicates the presence of abundant oxygen-containing surface groups (e.g., hydroxyl, carbonyl, and carboxylic moieties) and aromatic structures, while XRD and SEM (Figure 2) reveal a largely amorphous carbon matrix with graphitic domains and a porous morphology. The measured  $pH_{pzc}$  of LC ( $pH \approx 6$ ; Figure 3) and the weak pH dependence of dye removal between pH 3 and 8 indicate that, at the working pH 7.0, the LC surface is predominantly negatively charged, favoring electrostatic attraction with the cationic forms of CV and MB. In addition to this electrostatic contribution,  $\pi$ - $\pi$  stacking interactions between the aromatic rings of the dyes and the graphitic domains of LC, as well as possible hydrogen bonding between dye functional groups and surface oxygenated sites, are likely to play a role. The D-R adsorption energies ( $E < 8$  kJ mol<sup>-1</sup>; Table 1) and the temperature dependence of  $q_m$  and  $\Delta G^\circ$  (Table 3) point to a process dominated by physical adsorption, while the excellent fit of the pseudo-second-order kinetic model (Figure 6, Table 2) reflects the importance of surface interactions in controlling the overall rate. The somewhat stronger affinity observed for CV relative to MB under comparable conditions may be related to differences in molecular size, planarity, and charge distribution, which influence the balance of electrostatic and  $\pi$ - $\pi$  interactions with the LC surface.

While this study emphasizes the removal of synthetic

dyes, specifically CV and MB, the potential of LC extends beyond these applications. Biochar's porous structure and surface functional groups make it suitable for adsorbing a wide range of contaminants, including heavy metals, pharmaceuticals, and organic pollutants. Preliminary studies suggest that LC can effectively remove cadmium, lead, and arsenic ions from aqueous solutions, indicating its versatility as an adsorbent. In this work, LC was evaluated using synthetic single-dye solutions as a first step toward understanding its intrinsic adsorption behavior. Future studies should investigate the efficacy of LC in complex real water matrices, such as textile and mixed industrial wastewaters, and its potential for simultaneous removal of multiple pollutants. Additionally, an important practical consideration for any sorbent is its regenerability and service lifetime. In the present work, we did not perform systematic adsorption-desorption cycling experiments; our primary objective was to establish the intrinsic equilibrium, kinetic, and thermodynamic behavior of as-received LC toward CV and MB. Nevertheless, previous studies on citrus-derived biochars have shown that cationic dyes can be desorbed under mild alkaline or solvent treatment, with substantial retention of adsorption capacity over multiple cycles (Foroutan et al., 2021; Ramutshatsha-Makhwedzha et al., 2022; Mishra et al., 2023). Because regeneration efficiency and capacity retention directly determine the adsorbent cost per unit volume of treated water, future work will focus on quantifying LC reusability, mass loss, and energy input over repeated adsorption-desorption cycles, and on comparing these metrics with those of commercial activated carbon.

#### 4. Conclusions

The conversion of lemon peels into biochar offers a cost-effective, environmentally responsible alternative to conventional adsorbents such as activated carbon. Nevertheless, the overall environmental impact of biochar production warrants scrutiny, especially regarding the energy requirements for pyrolysis and the possible release of volatile organic compounds. Incorporating renewable energy sources, such as solar or biomass, could help mitigate these challenges and enhance sustainability. In addition, a comprehensive economic analysis comparing lemon-derived biochar with conventional adsorbents would inform large-scale adoption for water treatment applications. This investigation confirms that LC is highly effective for removing CV and MB from aqueous solutions. Characterization by FTIR, SEM, TGA, and XRD demonstrated the presence of functional groups, a porous microstructure, satisfactory thermal stability, and an amorphous nature, all of which are suitable for adsorption. Both dyes followed the Langmuir and Freundlich isotherm models, with kinetics aligning with a pseudo-second-order mechanism indicative of chemisorption. Thermodynamic analyses revealed that CV uptake is exothermic and spontaneous at lower temperatures, while MB adsorption is endothermic, showing increased spontaneity at higher temperatures. LC exhibited a distinctly higher partition coefficient for CV ( $K_d = 68.72$ ) than for MB ( $K_d = 2.75$ ), making it particularly useful in treatments involving mixed-dye pollutants. By repurposing waste materials, this approach advances multiple United Nations Sustainable Development Goals, including SDG 6 (Clean Water and Sanitation) and SDG 12 (Responsible Consumption and Production). Although regeneration experiments were not carried out in this study, the literature on citrus-derived biochars indicates that regeneration can be achieved with moderate energy inputs, which is essential for maintaining competitive treatment costs relative to commercial activated carbon (Foroutan et al., 2021; Ramutshatsha-Makhwedzha et al., 2022). Accordingly, future research should focus on pilot- and field-scale assessments that explicitly quantify LC regeneration efficiency, cycling-induced capacity loss, and the resulting cost per unit volume of treated water, in addition to evaluating long-term performance in complex wastewaters.

#### Acknowledgment

This work has been carried out by Fawwaz I. Khalili during a sabbatical leave from the University of Jordan, chemistry department, with the support of the Deanship of Scientific Research.

#### Statements and Declarations

##### Data Availability

The authors confirm that the data supporting the findings of this study are available within the article and its supplementary materials.

##### Disclosure statement

No potential conflict of interest was reported by the authors.

#### References

- Alam, M. S., Gorman-Lewis, D., Chen, N., Safari, S., Baek, K., Konhauser, K. O., & Alessi, D. S. (2018). Mechanisms of the removal of U(VI) from aqueous solution using biochar: A combined spectroscopic and modeling approach. *Environmental Science & Technology*, 52(22), 13057-67. <https://doi.org/10.1021/acs.est.8b01715>
- Al-Hosney, H. A., & Grassian, V. H. (2005). Water, sulfur dioxide, and nitric acid adsorption on calcium carbonate: A transmission and ATR-FTIR study. *Physical Chemistry Chemical Physics*, 7(6), 1266. <https://doi.org/10.1039/b417872f>
- Al-Jboor, M. M., & Khalili, F. I. (2011). Removal of nitrate ions from water using Jordanian lemon wood and olive seeds charcoal. *International Journal of Arts and Sciences*, 4(19), 283.
- Alnasra, O. A., & Khalili, F. I. (2023). Synthesis and characterization of a nanosilica-cysteine composite for arsenic(III) ion removal. *Acta Chimica Slovenica*, 70(4), 674-89. <https://doi.org/10.17344/acs.2023.8160>
- Al-Qadri, F., Abdulrahman, J., Yahia, A., & Faleh, N. (2024). Bio adsorbent lemon peels charcoal to remove Fe(III) from water sources. *Interciencia*, 32(1), 3-20. <https://doi.org/10.59671/Ch5fn>
- Ankona, E., Multanen, V., Nisnevitch, M., Billig, M., & Anker, Y. (2021). Investigation of pyrolysis kinetics and gaseous compounds emitted during charcoal production from woods commonly used in the eastern Mediterranean. *Biofuels, Bioproducts and Biorefining*, 15(3), 646-56. <https://doi.org/10.1002/bbb.2188>
- Azadian, M., & Gilani, H. G. (2023). Adsorption of Cu<sup>2+</sup>, Cd<sup>2+</sup>, and Zn<sup>2+</sup> by engineered biochar: Preparation, characterization, and adsorption properties. *Environmental Progress & Sustainable Energy*, 42(4), 14088. <https://doi.org/10.1002/ep.14088>
- Baloo, L., Isa, M. H., Sapari, N. B., Jagaba, A. H., Wei, L. J., Yavari, S., Razali, R., & Vasu, R. (2021). Adsorptive removal of methylene blue and acid orange 10 dyes from aqueous solutions using oil palm wastes-derived activated carbons. *Alexandria Engineering Journal*, 60(6), 5611-29. <https://doi.org/10.1016/j.aej.2021.04.044>
- Singh, B. J., Chakraborty, A., & Sehgal, R. (2023). A systematic review of industrial wastewater management: Evaluating challenges and enablers. *Journal of Environmental Management*, 348, 119230. <https://doi.org/10.1016/j.jenvman.2023.119230>
- Cheng, S., Zhao, S., Xing, B., Liu, Y., Zhang, C., & Xia, H. (2022). Preparation of magnetic adsorbent-photocatalyst composites for dye removal by synergistic effect of adsorption and photocatalysis. *Journal of Cleaner Production*, 348, 131301. <https://doi.org/10.1016/j.jclepro.2022.131301>
- Danish, M., Ahmad, T., Hashim, R., Said, N., Akhtar, M. N., Mohamad-Saleh, J., & Sulaiman, O. (2018). Comparison of surface properties of wood biomass activated carbons and their application against rhodamine B and methylene blue dye. *Surfaces and Interfaces*, 11, 1-13. <https://doi.org/10.1016/j.surfin.2018.02.001>
- Dittmann, D., Saal, L., Zietzschmann, F., Mai, M., Altmann, K., Al-Sabbagh, D., Schumann, P., Ruhl, A. S., Jekel, M., & Braun, U. (2022). Characterization of activated carbons for water treatment using TGA-FTIR for analysis of oxygen-containing functional groups. *Applied Water Science*, 12(8), 203. <https://doi.org/10.1007/s13201-022-01723-2>
- Dubinin, M. M. (1960). The potential theory of adsorption of gases and vapors for adsorbents with energetically non-uniform surfaces. *Chemical Reviews*, 60(2), 235-41. <https://doi.org/10.1021/cr60204a006>
- Foo, K. Y., & Hameed, B. H. (2012). Coconut husk derived activated carbon via microwave-induced chemical activation: Effects of activation agents on porous structure. *Journal of*

- Hazardous Materials, 190, 8-14. <https://doi.org/10.1016/j.cej.2011.12.084>
- Foroutan, R., Peighambaroust, S. J., Peighambaroust, S. H., Pateiro, M., Lorenzo, J. M. (2021). Adsorption of Crystal Violet dye using activated carbon of lemon wood and activated carbon/Fe<sub>3</sub>O<sub>4</sub> magnetic nanocomposite from aqueous solutions: A kinetic, equilibrium, and thermodynamic study. *Molecules*, 26(8), 2241. <https://doi.org/10.3390/molecules2608224>
- Freundlich, H. M. F. (1906). Over the adsorption in solution. *The Journal of Physical Chemistry A*, 57(385), 1100-7.
- Gabhi, R., Basile, L., Kirk, D. W., Giorcelli, M., Tagliaferro, A., Jia, C. Q. (2020). Electrical conductivity of wood biochar monoliths and its dependence on pyrolysis temperature. *Biochar*, 2(3), 369-78. <https://doi.org/10.1007/s42773-020-00056-0>
- Gomide, R. A. C., De Oliveira, A. C. S., Rodrigues, D. A. C., De Oliveira, C. R., De Assis, O. B. G., Dias, M. V., & Borges, S. V. (2020). Development and characterization of lignin microparticles for physical and antioxidant enhancement of biodegradable polymers. *Journal of Polymers and the Environment*, 28(4), 1326-34. <https://doi.org/10.1007/s10924-020-01685-z>
- Gugushe, A. S., Mpupa, A., Munonde, T. S., Nyaba, L., & Nomngongo, P. N. (2021). Adsorptive removal of Cd, Cu, Ni, and Mn from environmental samples using Fe<sub>3</sub>O<sub>4</sub>-ZrO<sub>2</sub>@APS nanocomposite: Kinetic and equilibrium isotherm studies. *Molecules*, 26(11), 3209. <https://doi.org/10.3390/molecules26113209>
- Gupta, V. K., & Suhas, (2009). Application of low-cost adsorbents for dye removal—a review. *Journal of Environmental Management*, 90(8), 2313-42. <https://doi.org/10.1016/j.jenvman.2008.11.017>
- Gupta, A., Sharma, V., Sharma, K., Kumar, V., Choudhary, S., Mankotia, P., Kumar, B., Mishra, H., Moulick, A., Ekielski, A., & Mishra, P. K. (2021). A review of adsorbents for heavy metal decontamination: Growing approach to wastewater treatment. *Materials*, 14(16), 4702. <https://doi.org/10.3390/ma14164702>
- Hasan, M. N., Shenashen, M. A., Hasan, M. M., Znad, H., & Awual, M. R. (2021). Assessing cesium removal from wastewater using functionalized wood cellulosic adsorbent. *Chemosphere*, 270, 128668. <https://doi.org/10.1016/j.chemosphere.2020.128668>
- Ibrahim, A., Fawal, G., & Akl, M. (2019). Methylene blue and crystal violet dyes removal (as a binary system) from aqueous solution using local soil clay: Kinetics study and equilibrium isotherms. *Egyptian Journal of Chemistry*, 62(3), 541-554. <https://doi.org/10.21608/ejchem.2018.4113.1360>
- Janu, R., Mrlik, V., Ribitsch, D., Hofman, J., Sedláček, P., Bielská, L., & Saja, G. (2021). Biochar surface functional groups as affected by biomass feedstock, biochar composition, and pyrolysis temperature. *Carbon Resources Conversion*, 4, 36-46. <https://doi.org/10.1016/j.crcon.2021.01.003>
- Kalina, M., Sovova, S., Hajzler, J., Kubikova, L., Trudicova, M., Smilek, J., & Enev, V. (2022). Biochar texture—a parameter influencing physicochemical properties, morphology, and agronomical potential. *Agronomy*, 12(8), 1768. <https://doi.org/10.3390/agronomy12081768>
- Kar, K. K. (2020). *Handbook of Nanocomposite Supercapacitor Materials I: Characteristics*. Springer Cham, Switzerland. <https://doi.org/10.1007/978-3-030-43009-2>
- Kütahyalı, C., & Eral, M. (2010). Sorption studies of uranium and thorium on activated carbon prepared from olive stones: Kinetic and thermodynamic aspects. *Journal of Nuclear Materials*, 396(2-3), 251-6. <https://doi.org/10.1016/j.jnucmat.2009.11.018>
- Langmuir, I. (1918). The adsorption of gases on plane surfaces of glass, mica, and platinum. *J Journal of the American Chemical Society*, 40(9), 1361-403. <https://doi.org/10.1021/ja02242a004>
- Li, J., Li, Y., Wu, Y., & Zheng, M. A. (2014). Comparison of biochars from lignin, cellulose, and wood as the sorbent to an aromatic pollutant. *Journal of Hazardous Materials*, 280:450-7. <https://doi.org/10.1016/j.jhazmat.2014.08.033>
- Li, Q., Ma, X., Hu, C., & Zhai, J. (2016). Removal of methylene blue from aqueous solution with magnetite loaded multi-walled carbon nanotube: Kinetics, isotherms, and thermodynamics. *Journal of Industrial and Engineering Chemistry*, 39, 93-101.
- Mariño, M., Lopes Da Silva, L., Durán, N., & Tasic, L. (2015). Enhanced materials from nature: Nanocellulose from citrus waste. *Molecules*, 20(4), 5908-23. <https://doi.org/10.3390/molecules20045908>
- Mishra, A., Ojha, H., Pandey, J., Tiwari, A. K., & Pathak, M. (2023). Adsorption characteristics of magnetized biochar derived from Citrus limetta peels. *Heliyon*, 9(10), e20665. <https://doi.org/10.1016/j.heliyon.2023.e20665>
- Mpupa, A., Nqombolo, A., Mizaikoff, B., & Nomngongo, P. N. (2020). Enhanced adsorptive removal of  $\beta$ -Estradiol from aqueous and wastewater samples by magnetic nano-Akaganeite: Adsorption isotherms, kinetics, and mechanism. *Processes*, 8(9), 1197. <https://doi.org/10.3390/pr8091197>
- Nuhanović, M., Grebo, M., Draganović, S., Memić, M., & Smječanin, N. (2019). Uranium(VI) biosorption by sugar beet pulp: Equilibrium, kinetic and thermodynamic studies. *Journal of Radioanalytical and Nuclear Chemistry*, 322(3), 2065-78. <https://doi.org/10.1007/s10967-019-06877-z>
- Oruç, Z., Ergüt, M., Uzunoğlu, D., & Özer, A. (2019). Green synthesis of biomass-derived activated carbon/Fe-Zn bimetallic nanoparticles from lemon (Citrus limon (L.) Burm. f.) wastes for heterogeneous Fenton-like decolorization of Reactive Red 2. *Journal of Environmental Chemical Engineering*, 7(4), 103231. <https://doi.org/10.1016/j.jece.2019.103231>
- Öztürk, N., & Bektaş, T. E. (2004). Nitrate removal from aqueous solution by adsorption onto various materials. *Journal of Hazardous Materials*, 112(1-2), 155-62. <https://doi.org/10.1016/j.jhazmat.2004.05.001>
- Pérez, S., Ulloa, M., Flórez, E., Acelas, N., Ocampo-Pérez, R., Padilla-Ortega, E., & Forgiionny, A. (2023). Valorization of lemon peel wastes into a potential adsorbent for simultaneous removal of copper ion (Cu<sup>2+</sup>) and Congo red from wastewater. *Environmental Nanotechnology, Monitoring & Management*, 20, 100795. <https://doi.org/10.1016/j.enmm.2023.100795>
- Poonam, & Kumar, N. (2020). Experimental and kinetic study of removal of lead (Pb<sup>2+</sup>) from battery effluent using sweet lemon (Citrus limetta) peel biochar adsorbent. *Environment, Development and Sustainability*, 22(5), 4379-406. <https://doi.org/10.1007/s10668-019-00389-2>
- Ramutshatsha-Makhwedzha, D., Mavhungu, A., Moropeng, M., & Mbaya, R. (2022). Activated carbon derived from waste orange and lemon peels for the adsorption of methyl orange and methylene blue dyes from wastewater. *Heliyon*, 8(8), e09930. <https://doi.org/10.1016/j.heliyon.2022.e09930>
- Roy, H., Prantika, T. R., Riyad, M. H., Paul, S., & Islam, M. S. (2022). Synthesis, characterizations, and RSM analysis of Citrus macroptera peel-derived biochar for textile dye treatment. *South African Journal of Chemical Engineering*, 41, 129-39. <https://doi.org/10.1016/j.sajce.2022.05.008>
- Rožič, M., Senji, I., & Miljanić, S. (2014). Methylene blue sorption characterization onto orange and lemon peels. *The Holistic Approach to Environment*, 4(3), 97-110.
- Šabanović, E., Muhić-Šarac, T., Nuhanović, M., & Memić, M. (2019). Biosorption of uranium(VI) from aqueous solution by Citrus limon peels: Kinetics, equilibrium, and batch studies. *Journal of Radioanalytical and Nuclear Chemistry*, 319(1), 425-35. <https://doi.org/10.1007/s10967-018-6358-3>
- Saeed, A., Sharif, M., & Iqbal, M. (2010). Application potential of grapefruit peel as dye sorbent: Kinetics, equilibrium and mechanism of Crystal Violet adsorption. *Journal of*

Hazardous Materials, 179, 564-72. <https://doi.org/10.1016/j.jhazmat.2010.03.041>

Senophiyah-Mary, J., Thomas, T., Loganath, R., & Meenambal, T. (2019). Removal of copper from bioleachate of e-waste using lemon activated carbon (LAC) and comparison with commercial activated carbon (CAC). In: Ghosh SK (ed) Waste Valorisation and Recycling. Springer, Singapore, pp 385-395. [https://doi.org/10.1007/978-981-13-2784-1\\_36](https://doi.org/10.1007/978-981-13-2784-1_36)

Senthilkumar, S., Varadarajan, P. R., Porkodi, K., Subbhuraam, C. V. (2005). Adsorption of methylene blue onto jute fiber carbon: Kinetics and equilibrium studies. *Journal of Colloid and Interface Science*, 284, 78-82. <https://doi.org/10.1016/j.jcis.2004.09.027>

Sirico, A., Bernardi, P., Sciancalepore, C., Vecchi, F., Malcevski, A., Belletti, B., & Milanese, D. (2021). Biochar from wood waste as an additive for structural concrete. *Construction and Building Materials*, 303, 124500. <https://doi.org/10.1016/j.conbuildmat.2021.124500>

Stella Mary, G., Sugumaran, P., Niveditha, S., Ramalakshmi, B., Ravichandran, P., & Seshadri, S. (2016). Production, characterization, and evaluation of biochar from pod (*Pisum sativum*), leaf (*Brassica oleracea*), and peel (*Citrus sinensis*) wastes. *International Journal of Recycling of Organic Waste in Agriculture*, 5(1), 43-53. <https://doi.org/10.1007/s40093-016-0116-8>

Stevens, R. W., Siriwardane, R. V., & Logan, J. (2008). In situ Fourier Transform Infrared (FTIR) investigation of CO<sub>2</sub> adsorption onto zeolite materials. *Energy Fuels*, 22(5), 3070-9. <https://doi.org/10.1021/ef800209a>

Surya, K., & Michael, M. S. (2021). Hierarchical porous activated carbon prepared from biowaste of lemon peel for electrochemical double-layer capacitors. *Biomass Bioenergy*, 152, 106175. <https://doi.org/10.1016/j.biombioe.2021.106175>

Temkin, M. I., & Pyzhev, V. (1940). Kinetics of Ammonia Synthesis on Promoted Iron Catalysts. *Acta Physicochim*, 12, 327-356.

Tintner, J., Preimesberger, C., Pfeifer, C., Soldo, D., Ottner, F., Wriessnig, K., Rennhofer, H., Lichtenegger, H., Novotny, E. H., & Smidt, E. (2018). Impact of pyrolysis temperature on charcoal characteristics. *Industrial & Engineering Chemistry Research*, 57(46), 15613-9. <https://doi.org/10.1021/acs.iecr.8b04094>

Wang, T., Tang, X., Zhang, S., Zheng, J., Zheng, H., & Fang, L. (2019). Roles of functional microbial flocculant in dyeing wastewater treatment: Bridging and adsorption. *Journal of Hazardous Materials*. 384, 121506. <https://doi.org/10.1016/j.jhazmat.2019.121506>

Xie, Z., Guan, W., Ji, F., Song, Z., & Zhao, Y. (2014). Production of biologically activated carbon from orange peel and landfill leachate subsequent treatment technology. *Journal of Chemistry*, 1-9. <https://doi.org/10.1155/2014/491912>